Effects of Photodeposited Au vs. Pt Nanoparticles on N,F-doped TiO_2 Photoactivity: a Time-resolved Photoluminescence Investigation

Maria Vittoria Dozzi,[,†] Alessia Candeo,[‡] Gianluigi Marra,[§] Cosimo D'Andrea,[‡,#] Gianluca Valentini,[‡] and Elena Selli[†]*

[†] Dipartimento di Chimica, Università degli Studi di Milano, via Golgi 19, I-20133 Milano, Italy

[‡] IFN-CNR, Dipartimento di Fisica, Politecnico di Milano, Piazza Leonardo da Vinci 32, I-20133 Milano, Italy

[§] Renewable Energy and Environmental R&D, Istituto Eni Donegani, Via Fauser 4, I-28100 Novara, Italy

[#] Center for Nano Science and Technology@PoliMi, Istituto Italiano di Tecnologia, Via Giovanni Pascoli 70/3, 20133 Milano, Italy

* Corresponding Author. Tel. +39 02 50314298; Fax: +39 02 50314300; e-mail: mariavittoria.dozzi@unimi.it.

ABSTRACT: The time-resolved photoluminescence (PL) in the nanosecond time scale of TiO_2 materials undoped or co-doped with nitrogen and fluorine (N,F-doping) and modified by noble metals (NM, *i.e.* Au or Pt) nanoparticles (NPs) photodeposition has been systematically investigated in relation to their photocatalytic activity in hydrogen production. Main aim of the study is to elucidate the origin of the NM-dependent synergistic effects in photoactivity produced by N,F-doping of TiO_2 and NM NPs deposition on the oxide surface. While TiO_2 doping with fluorine and nitrogen introduces new stabilized luminescent defective trap states below the conduction band revealed by long-living PL components, the presence of NM NPs on the TiO_2 surface produces a PL intensity suppression, which is more relevant for Au- rather than for Pt-NPs containing materials. Time resolved PL analysis indicates that the electron transfer occurring at the TiO_2/metal interface is affected by both the defective structure of anatase N,F-doped TiO_2 and the type of NM (Au or Pt). In particular, Au rather than Pt NPs appear to strongly interact with the charge carriers trapped at surface defect sites, gold NPs being expected to preferentially grow on such sites during photodeposition. Furthermore, plasmonic gold NPs excitation upon PL light absorption is evidenced by the PL spectral shape variation observed only in the case of Au/TiO_2. Thus the larger synergistic effect on photocatalytic hydrogen production observed upon Au NPs photodeposition on N,F-doped TiO_2 results from the opening of a new efficient electron transfer path from luminescent defective trap states on doped TiO_2 to Au NPs, where proton reduction occurs.

1. INTRODUCTION

In order to boost the photocatalytic performance of TiO_2, the most largely employed, stable and cost-effective photocatalyst, a wide variety of strategies has been employed, aimed either at enhancing its ability to absorb light, or at improving the separation of the charge couples photogenerated in it upon light absorption.[1–3] In particular, the insertion of dopant species in the oxide, eventually accompanied by the introduction of defective sites such as oxygen vacancies, may produce extra UV-visible light absorption, which, however, does not necessarily guarantee an effectively increased photoactivity.[4] In fact, an excess of newly created mid-gap energy and/or defective states may enhance the rate of the undesired recombination of photogenerated charge carriers, with detrimental effects on the photoefficiency of bulk-modified TiO_2 systems.[5]

Further photoactivity enhancement can be obtained by coupling an optimized level of TiO_2 doping with the deposition of noble metal (*i.e.* Pt, Au, Pd) nanoparticles (NPs) on the semiconductor surface. These latter, in fact, act as efficient scavengers of photoexcited electrons due to the equilibration of the Fermi level in both metal and semiconductor components, with consequent band bending in TiO_2 and formation of a Schottky barrier at the semiconductor-metal junction, which ensures a more efficient electron-hole separation.[6,7]

In this context, among various advanced characterization techniques able to track the separation of photoproduced charge carriers in both space and time domains,[8] photoluminescence (PL), resulting from the radiative electron-hole recombination path and usually weak in the case of TiO_2, has also been employed. The shape and intensity of the PL emission of pure TiO_2 has been investigated mainly in relation to its crystalline phase composition[9–11] or morphology.[12,13] TiO_2 PL was found to be sensitive to both the synthesis method and to specific post synthesis treatments under aerobic or anaerobic conditions,

introducing near-surface defect states,[14,15] as well as to electron donor or acceptor species adsorbed on the oxide surface.[16–18]

In a previous investigation[19] we demonstrated that doping TiO_2 with fluorine and nitrogen (N,F-doping) plays a key role in introducing new components in the PL emission of TiO_2 and affects the dynamics of the charge carriers generated upon band gap excitation under conditions similar to those adopted in photocatalytic reactions. Specifically, by time-resolved PL spectroscopy a clear correlation was outlined between the long-lasting PL decay component and the photocatalytic performance of N,F-doped TiO_2-based materials.[19] Thus, long-living surface defect trap states may improve the separation efficiency of photogenerated electron-hole couples, with an overall positive effect on photoactivity.

On the other hand, we also found that N,F-doping of TiO_2 synergistically increases the well-established beneficial effect of noble metal (NM) NPs on the TiO_2 surface, especially in the photoreduction path leading to H_2 production from water solutions.[20] Aiming at clarifying if and how the mechanism of electron transfer from the conduction band (CB) of the photoexcited semiconductor to the NM NPs may be affected by the type of NM (Au or Pt) and/or by the peculiar defective structure of N,F-doped TiO_2 materials, in the present work we investigate the time-resolved PL (in the nanosecond time scale) upon excitation at 355 nm of Au- or Pt-modified N,F-doped TiO_2 photocatalyst samples, in comparison with that of either doped or undoped bare materials and in relation to their photocatalytic activity in hydrogen production from aqueous methanol solutions.

2. EXPERIMENTAL SECTION

2.1. Synthesis and surface modification of doped TiO_2 powders. The doped titania photocatalysts (D-TiO_2) were prepared by the sol-gel method in the presence of different amounts of NH_4F dopant source and then calcined at 700 °C, as already described.[4,21] They

were labeled as D_X, with X referring to the nominal dopant/Ti percent molar ratio (X = 5 and 12). XPS analysis confirmed the presence of both N and F, mainly in the substitutional and surface forms, respectively, increasing with increasing nominal dopant amount.[4] A reference undoped material, named D_0, was prepared by exactly the same synthetic route in the absence of dopant.

NM NPs-modified TiO_2 samples were obtained as already detailed,[20] by photodeposition from methanol/water suspensions containing the amount of $HAuCl_4$ or H_2PtCl_6 (in the case of gold and platinum NPs deposition, respectively) necessary to obtain a nominal metal loading of 0.5 wt.%. This NM loading of TiO_2 was found to be optimal, being the best balance between the shielding effects of NM surface NPs, decreasing the fraction of light absorbed by TiO_2, and their beneficial role in capturing CB electrons, thus reducing the recombination of photoproduced electron-hole couples.[22,23] NM-modified samples were labelled as NM/D_X, where NM refers to Au or Pt deposited NPs. Quantitative deposition of the NMs was confirmed by ICP analysis.[20] Moreover, the presence of a similar amount of Au and Pt on the surface of all here investigated materials was further assessed by X-ray fluorescence (XRF) analysis employing a Elio XGlab spectrometer.

2.2. Photocatalysts characterization and photoactivity tests. X-ray powder diffraction (XRPD) patterns were recorded on a Philips PW3020 powder diffractometer, by using the Cu Kα radiation (λ = 1.54056 Å).[21,24] Anatase crystallite dimensions were calculated by applying the Scherrer equation to the most intense anatase peak of each XRPD pattern. BET specific surface area analysis was performed by N_2 adsorption/desorption at liquid nitrogen temperature in a Micromeritics ASAP 2010 apparatus, after out-gassing in vacuo at 300 °C for at least 6 h.

UV-Vis diffuse reflectance (DR) spectra were recorded with a Lambda 19, Perkin Elmer spectrophotometer equipped with an integrating sphere and then converted into absorption (A) spectra (A = 1 – R).[4,20]

HR-TEM analysis was carried out with a JEOL JM 2010 electron microscope, equipped with a LAB6 electron gun operating at 200 keV and a Gatan CCD camera allowing high-resolution imaging. Few (2-3) milligrams of powders for HR-TEM analysis were sonicated in 2-propanol and then transferred as a suspension to a copper grid covered with a holey carbon film.

The photocatalytic activity tests of the investigated photocatalyst powders in hydrogen production by methanol photosteam reforming were performed under nitrogen atmosphere in a closed recirculation laboratory scale apparatus, as detailed elsewhere.[24] Briefly, the photoreactor consisted in a flat cylindrical Plexiglass cell, containing the photocatalyst powder deposited on quartz beads. This photocatalyst bed was continuously fed with a stream of N_2 saturated with the vapor of a 20 vol.% methanol-water solution thermostated at 30 °C, and irradiated with a xenon lamp with a full irradiation intensity of 0.31 W cm^{-2}. During the runs, the recirculating gas was automatically sampled on-line and injected into a gas chromatograph, the response of which was preliminary calibrated for H_2 analysis.

2.3. Time-resolved photoluminescence spectroscopy and data analysis. Emission lifetime measurements were performed using a time resolved spectroscopy system based on a pulsed laser and a fast-gated detector. The excitation light was provided by the third harmonic of a Nd:YAG laser, in Q-switch regime, emitting sub-ns pulses at 355 nm (CryLas FTSS 355-50-779) with 100 Hz repetition rate. The measurements were performed after fixing each sample, in the form of circular pellet of powder (1 cm diameter), on an aluminum sample holder. The fluorescence emission was collected and focused to the entrance slit of an imaging spectrometer (SP2300, Princeton Instruments, USA) that enabled us to record the

emission spectrum from 400 nm to 720 nm, with a resolution of *ca.* 3 nm. The exit port of the spectrometer was coupled to a time-gated image intensifier (C9546-03, Hamamatsu Photonics, Japan), featuring an acquisition gate adjustable from 3 ns to continuous mode. The light intensifier was optically coupled to a low noise, 1280 x 1024 pixel, CCD camera (Retiga R6, QImaging, Canada), which records the wavelength dispersed luminescent emission. The synchronization of the gated intensifier with the laser pulses was provided by a homemade circuit coupled to a precision delay generator (DG535, Stanford Research Systems, Sunnyvale, CA). The jitter of the system, which sets the overall time resolution, is very small (< 250 ps) and significantly lower than the rising edge of the acquisition gate. For the measurements, the gate width was set to 10 ns and a sequence of delayed spectra was taken with uneven temporal spacing between delays. A first sequence of delayed spectra was acquired with 1 ns relative spacing, starting from a null delay (leading edge of the gate synchronous with the laser pulse) to a delay of 13 ns; then, a 5 ns spacing between delay was adopted up to 113 ns; finally, a sequence of delayed spectra was acquired with 40 ns relative spacing. The uneven temporal sampling was adopted in order to account for the different decay times of the emission components. A total of 60 spectra, including some background spectra taken at very long delays (milliseconds), were acquired for each sample. The whole measurement procedure took about 3 min per sample and was repeated in the same way for all of them. Yet, for several samples the long-delay spectra were dropped from the analysis due to lack of signal.

The dataset represents the dynamic behavior of the emission as a function of time. Each element of this dataset was fitted to recover the amplitude and lifetime of three emission components, using the following model:

$$F(d) = A_1 \tau_1 \mathrm{e}^{-\frac{d}{\tau_1}} \left(1 - \mathrm{e}^{-\frac{W}{\tau_1}}\right) + A_2 \tau_2 \mathrm{e}^{-\frac{d}{\tau_2}} \left(1 - \mathrm{e}^{-\frac{W}{\tau_2}}\right) + A_3 \tau_3 \mathrm{e}^{-\frac{d}{\tau_3}} \left(1 - \mathrm{e}^{-\frac{W}{\tau_3}}\right) + W\,Offset$$

where F is the fluence, *i.e.* the integral of the emission intensity within the gate window, d is the acquisition delay for each data point of the sequence, while A_i and τ_i (i = 1, 2, 3) are the amplitude and lifetime of each emission component. The terms $[1-\exp(-W/\tau_i)]$ are required to correct for the finite width (W) of the sampling window (10 ns).

The fitting method is based on a standard least mean square algorithm derived from the math library provided by the Numerical Algorithms Group. More details on the PL experimental setup (see Figure S1 in the Supporting Information) and on the fitting method (see Figure S2) are provided elsewhere.[25]

3. RESULTS AND DISCUSSION

3.1 Photocatalysts characterization. Quantitative phase analysis based on the XRPD patterns[21,24] confirmed that doped D_X materials (X = 5, 12), though having been calcined at 700 °C, consisted of almost pure anatase, while undoped D_0 was a rutile and anatase mixture (see Table 1). This is in line with previous findings clearly demonstrating that doping TiO_2 with nitrogen and fluorine inhibits the anatase into rutile phase transition, usually occurring when pure anatase is heated above 600 °C.[20]

.

Table 1. Phase composition and anatase crystallite dimensions, d_A, of the D_X photocatalysts, obtained from XRPD analysis by assuming the absence of amorphous phase; and their specific surface area (SSA), obtained from BET analysis.

Sample	Anatase (%)	Rutile (%)	d_A /nm	SSA/m^2 g^{-1}
D_0	38	62	65	7
D_5	99	1	49	16
D_12	99	1	48	12

The specific surface area of doped materials was slightly larger with respect to that of the corresponding undoped TiO_2, as reported in Table 1. Furthermore, gold or platinum NPs photodeposition on the TiO_2 samples, leading to a color change from white into purple or grey, respectively, did not affect their phase composition and surface area, as already found in previous studies.[20,22]

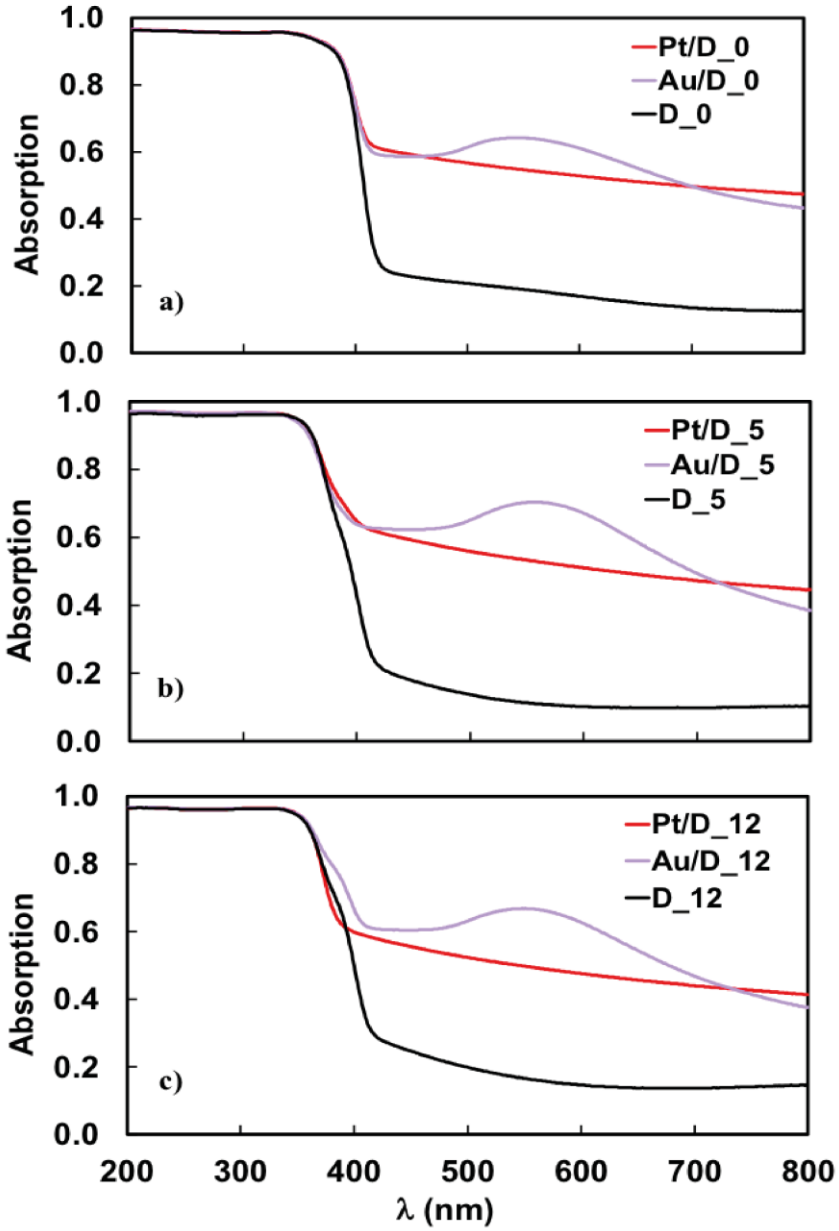

Figure 1. Absorption spectra of the (a) NM/D_0, (b) NM/D_5 and (c) NM/D_12 photocatalysts series (NM = Au or Pt).

As shown in Figure 1, all Au/D_X materials display the typical plasmon resonance absorption band, with a maximum around 550 nm, while Pt/D_X samples exhibit a broad absorption extending over the entire visible region. No appreciable difference is observed in the maximum position of the plasmonic band of Au/D_X samples. In fact, due to the pretty similar anatase TiO_2 particle sizes of bare D_X samples, no strong variation in size of the photodeposited Au NPs is expected, whereas an appreciable red-shift of the maximum plasmonic absorption would have been observed in the case of a significant enlargement of Au NPs size.[26,27]

HR-TEM analysis (see Figures 2 and 3) clearly demonstrates that both the size and the distribution of Au and Pt NPs is strongly affected by the type of photodeposited noble metal. At first glance, Pt NPs photodeposited on D_0 and D_5 (Figure 2c,d) are significantly smaller than photodeposited Au NPs (Figure 2 a,b) and exhibit a larger dispersion level. Moreover, Au NPs photodeposited on moderately doped Au/D_5 are smaller than those photodeposited on undoped Au/D_0, their mean particle diameters being approximately 8 and 11 nm, respectively.

Furthermore, as better shown in Figure 3, moderate N,F-doping of TiO_2 ensures a more homogeneous and regular distribution of spherically shaped Au NPs, mainly characterized by a well-defined unimodal size (Figure 3a). A broader Au NPs size distribution is obtained in the case of Au/D_0 (Figure 3b), in line with the corresponding wider plasmonic absorption profile (Figure 1a), possibly enabling the visible light absorption in a more extended wavelength range. Differently, in the case of Pt-modified TiO_2, the mean size of Pt NPs is always *ca.* 2 nm, independent of N,F-doping (Figure 3c,d).

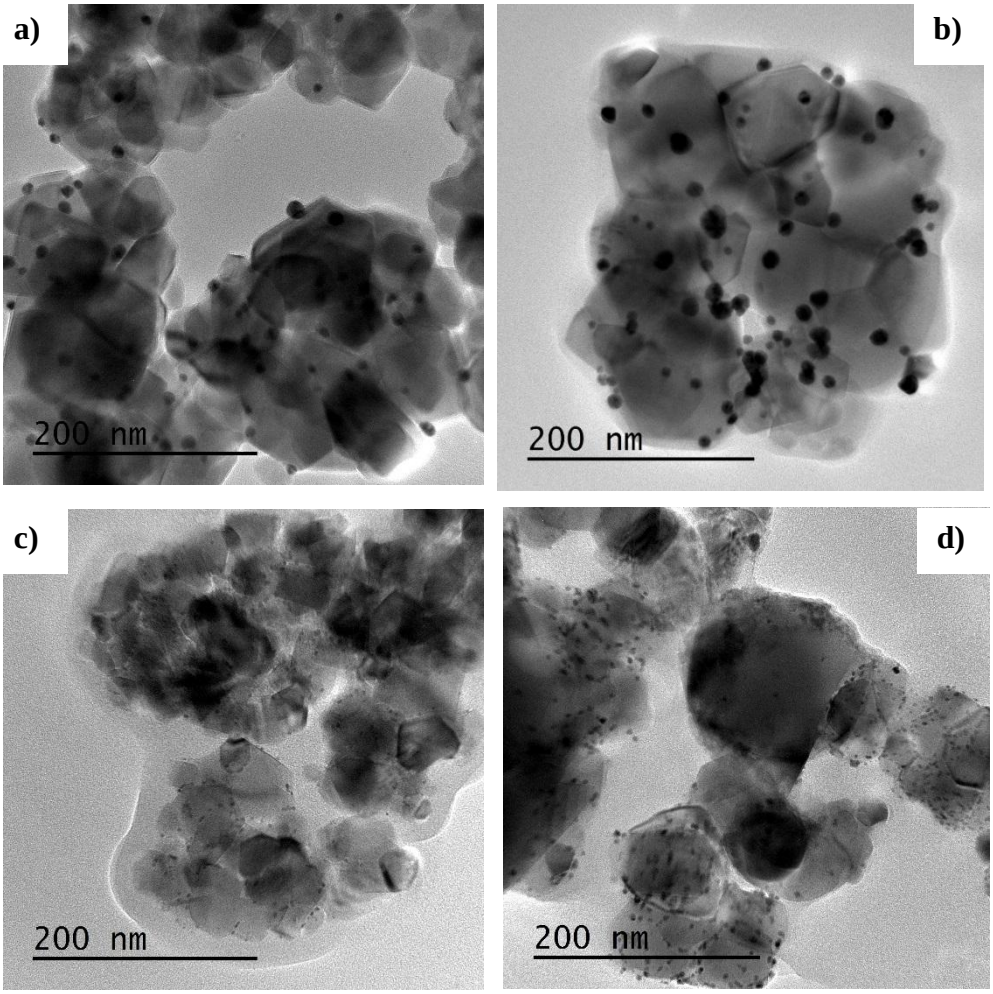

Figure 2. HR-TEM images of TiO_2 samples modified by NM NPs deposition: (a) Au/D_5; (b) Au/D_0; (c) Pt/D_5; (d) Pt/D_0.

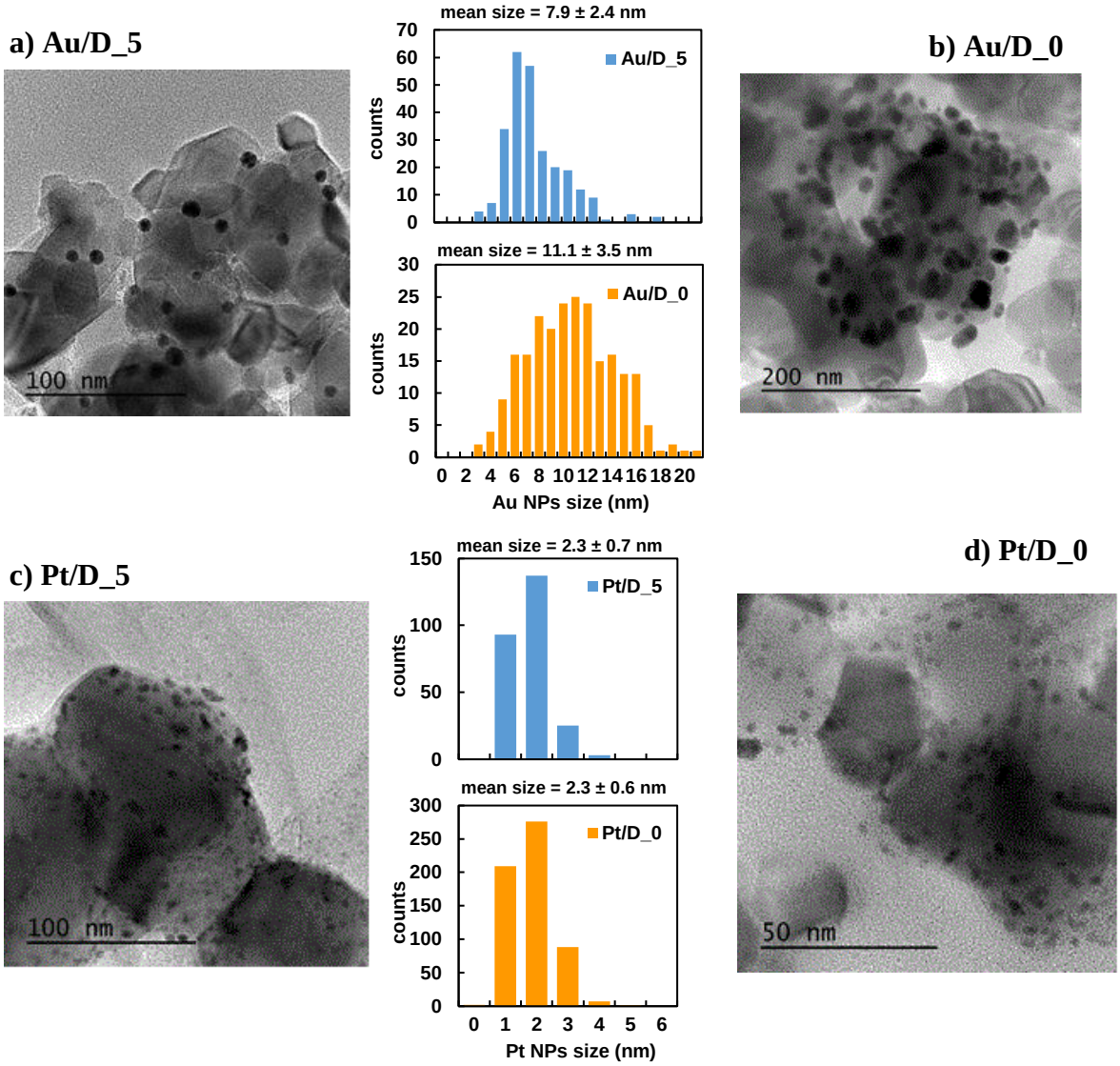

Figure 3. HR-TEM images and particle size distribution of (a) Au/D_5; (b) Au/D_0; (c) Pt/D_5; (d) Pt/D_0. Size distributions were calculated from HR-TEM images, by taking into account at least 250 NM NPs.

3.2 Photocatalytic production of H_2 by photo-steam reforming of methanol. Hydrogen evolution occurred at constant rate under irradiation as reported in Figure S3, in line with our previous studies.[24,28] Photoactivity was thus evaluated in terms of zero order rate constants *k*. No hydrogen production was observed under visible light irradiation (λ_{irr} > 420 nm), which rules out any appreciable contribution of Au plasmonic induced effects on photoactivity, as expected for such a low amount of photodeposited gold (0.5 wt.%).

In the case of Au- or Pt-modified TiO_2 the rate of hydrogen production in methanol photo-steam reforming was more than ten-fold higher than with the corresponding bare photocatalysts. Furthermore, the rate increase due to the NM NPs co-catalysts attained in this reaction was much more remarkable than that attained in formic acid photocatalytic oxidation.[20] Indeed, NM NPs on the semiconductor surface are confirmed to play a key role in capturing photopromoted CB electrons, with a consequent increased efficiency of photo-generated electron–hole pairs separation and interface electron transfer.

By considering the rate constant values of H_2 photocatalytic production collected in Table 2, Pt is a better co-catalyst than Au. This fact can be explained by the higher work function value of Pt (ϕ_{Pt} = 5.93 eV) with respect to that of Au (ϕ_{Au} = 5.31 eV), with the consequent formation of a higher Schottky barrier, generated by the band alignment at the metal–semiconductor hetero-junction, leading to a more efficient separation of the photoproduced charge carriers.

Table 2. Zero-order rate constants of H_2 photocatalytic production on un-modified D_X TiO_2, and on 0.5 wt% Au- or Pt-modified D_X TiO_2.

X F/Ti molar ratio (%)	k (mmol h^{-1} g_{cat}^{-1})		
	D_X	Au/D_X	Pt/D_X
0	0.13 ± 0.01	0.58 ± 0.02	3.0 ± 0.5
5	0.18 ± 0.01	3.8 ± 0.2	10.4 ± 0.8
12	0.14 ± 0.01	1.00 ± 0.02	2.68 ± 0.18

Actually, N,F-doping of TiO_2 produced negligible effects on the rate of H_2 evolution, the rate constant k values obtained with bare D_X photocatalysts being only slightly different with respect to that obtained with D_0. However, N,F-doping appears to determine the extent

of photocatalytic activity increase attained with NM-modified materials in comparison to the corresponding bare ones. The effects on photoactivity induced by NM NPs photodeposition on undoped and differently N,F-doped TiO_2 photocatalysts can better be evaluated in terms of the ratios between the H_2 production rate obtained with each NM/D_X sample (k_{Au} or k_{Pt}) and that achieved with the corresponding naked D_X one (k). These values are reported in Figure 4.

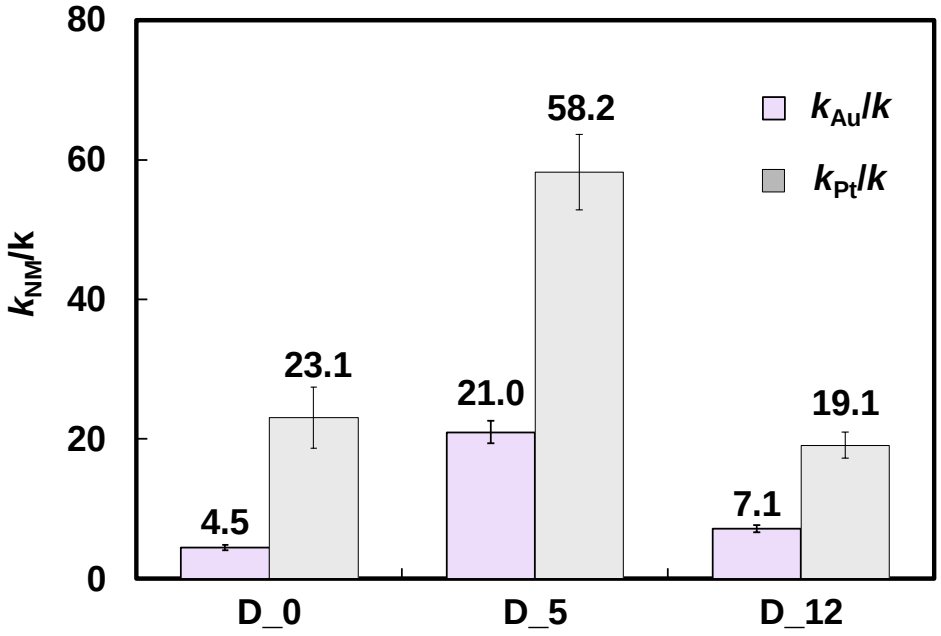

Figure 4. Ratios between the zero-order rate constants obtained with NM-modified samples (k_{NM}) and that obtained with the corresponding D_X sample (k).

The photoactivity increase determined by Pt or Au NPs deposition on D_5 was remarkably higher than that attained with undoped D_0 and doped D_12. Furthermore, doping seems to provide a relatively higher photoefficiency increase upon Au rather than Pt photodeposition. In fact, the k_{Pt}/k = 58.2 ratio obtained for Pt/D_5, though being the highest rate constant ratio attained upon NM NPs photodeposition on TiO_2 (Figure 4), is only *ca.* 2.5 times larger than the k_{Pt}/k = 23.1 ratio obtained with undoped D_0. In contrast, the k_{Au}/k = 21.0 ratio attained with Au/D_5 is *ca.* 5 times larger than the k_{Au}/k = 4.5 ratio obtained with undoped D_0.

Furthermore, by comparing the results obtained upon NM NPs deposition on D_12 with respect to undoped D_0, a rate increase is obtained upon gold NPs deposition on D_12, whereas a slight rate decrease is obtained when platinum NPs were deposited on D_12.

Thus, the combination of N,F-doping of TiO_2 with the subsequent photodeposition of NM NPs, and in particular of Au NPs, appears to produce an extra positive effect on photoactivity in the proton reduction path leading to H_2 evolution, with respect to NM NPs photodeposition on pure TiO_2. Similar, though less marked, synergistic effects were observed with Au-modified N,F-doped TiO_2 samples also in the photocatalytic mineralization of formic acid under UV-vis irradiation (see Figure S4).

3.3 Time resolved photoluminescence analysis. Time-resolved PL spectroscopy was thus performed to get information on the electron transfer paths from the excited semiconductor to the NM NPs, aiming at understanding the synergistic effects of the NM (Au or Pt) NPs and the peculiar structure of anatase N,F-doped TiO_2 materials. The PL signal of the Au or Pt-modified TiO_2 samples was compared with that of the corresponding either doped or undoped bare materials, in terms of intensity, shape and decay profile upon excitation at 355 nm.

By considering that TiO_2 is an indirect semiconductor, its emission signal resulting from the recombination of CB electrons with valence band (VB) holes is expected to be very weak at room temperature. However, such fast electron-hole recombination process, which largely occurs producing heat instead of radiative emission, is detrimental and strongly limits the photocatalytic efficiency of TiO_2-based materials. Differently, the introduction of localized defect states in the TiO_2 structure, *e.g.* by doping or by applying specific surface treatments under aerobic or anaerobic conditions, may produce trap sites of photogenerated charged species, resulting in slower relaxation pathways. These include the radiative recombination of trapped electrons and holes and electron transfer processes at the interface with a fluid phase, leading to beneficial effects on the overall photoactivity of the material.[29] Of course, if

photogenerated electrons or holes are efficiently trapped at specific defect sites, the probability that they interact with adsorbed oxidizable or reducible species largely increases,[11,30] with a parallel decrease of the undesired electron-hole recombination.

The steady state PL spectra of bare undoped D_0 and of doped D_5 and D_12 are shown in Figure 5. In line with our previous observation,[19] D_0 exhibits a low intensity PL signal in the 400-450 nm range, which may be assigned to the radiative recombination of bulk self-trapped excitons at intrinsic TiO_6 octahedra of anatase and rutile TiO_2 crystal structure.[15,31–33] Conversely, D_5 and D_12 exhibit more intense and broad PL signals, centered around 500 nm, *i.e.* red-shifted with respect to that of undoped D_0. The PL spectra of these two doped materials are equally shaped, that obtained from D_5 being somewhat more intense than that of D_12.

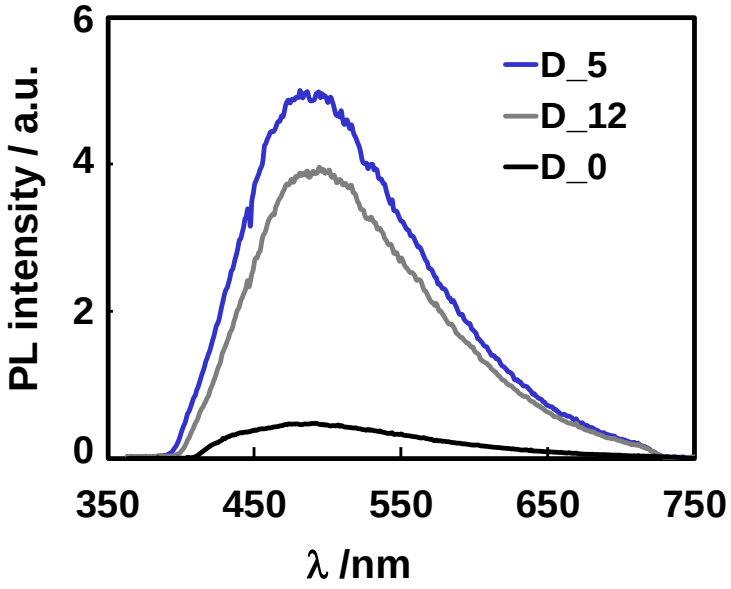

Figure 5. Photoluminescence spectra of D_0 (black trace), D_5 (blue trace) and D_12 (grey trace) upon excitation at 355 nm.

Thus, N,F doping of titania introduces a new range of intra band gap states, mainly leading to the formation of Ti^{3+} centers, possibly ascribed to oxygen vacancies[34] or consequent to the insertion of fluorine in the TiO_2 matrix.[35] These centers work as trapping sites of

photoproduced charge carriers, thus significantly affecting the overall electron−hole recombination dynamics. In fact, electron−hole recombination taking place between Ti^{3+} trap states (localized just a few tenths of an electronvolt below the bottom of the CB) and VB holes represents the most reasonable scheme to account for the PL response for the here investigated N,F-codoped TiO_2 materials, which also justifies the observed red-shift in the PL maximum with respect to pure TiO_2.[19] Thus both D_5 and D_12 display surface defect sites originating a more intense and longer living PL component, which is almost absent in the PL emission of D_0, as already discussed elsewhere[19] and here confirmed by time-resolved PL analysis (see Table 3).

The effects induced on the PL response by the presence of NM (*i.e.* Au or Pt) NPs on the TiO_2 surface can be appreciated in Figure 6. All NM/D_X samples exhibit a PL emission similar in shape to that originated by the corresponding unmodified D_X material, though less intense. This is due to a lower density of long living electron-hole couples consequent to the migration of photopromoted electrons into the NM NPs.[14,16,17,36–39] A new nonradiative electron transfer channel is thus opened, with a consequent reduction of the long living luminescence from the modified TiO_2 materials. No extra PL component was shown by our NM/D_X samples, differently from what recently reported by Jana *et al.* and attributed to combined fluorescence resonance energy transfer (FRET) and surface plasmon resonance (SPR) effects.[40] This confirms that NM NPs may efficiently capture photoexcited electrons from TiO_2, providing a recombination route for the holes in TiO_2 particles that does not generate PL, in line with the results of surface photovoltage measurements performed on Au/TiO_2 systems by Stevanovic *et al.*[36]

Interestingly, as shown in Figure 6a, in the case of undoped D_0, which is almost free of PL emitting surface defective sites, as confirmed by its extremely low PL emission, the presence of Pt NPs produces a larger PL decrease than Au NPs. In contrast, the decrease of

PL intensity is much more remarkable when Au NPs, rather than Pt NPs, are deposited on doped TiO_2 (see Figure 6), and in particular in the case of Au/D_5, which also exhibits the highest relative photoactivity increase upon NM NPs deposition (Table 2 and Figure 4). Au, rather than Pt NPs thus seem to efficiently interact with the photopromoted electrons trapped at the specific defect sites in doped TiO_2 which are responsible for the long-lasting PL emission. A possible explanation of this effect is that such trap states may selectively mediate the transfer of photopromoted electrons towards photodeposited Au NPs, while this electron transfer path appears to be relatively minor in the case of Pt NPs, electron transfer to Pt NPs mainly occurring directly from the TiO_2 CB.

The evidence of a significant interaction between Au NPs and electrons trapped at the defect sites of N,F-codoped TiO_2 is also testified by the relatively slight but peculiar change in spectral shape of the PL response, which was observed only in the case of Au NPs containing doped materials (*i.e.* Au/D_5 and Au/D_12), not in the case of undoped NM/D_0 (see insets of Figure 6). In fact, the normalized PL spectrum of Au/D_5 shows a remarkably lower emission in the 500-600 nm range compared to that of bare D_5, which perfectly matches the plasmonic absorption features of Au NPs on TiO_2 (compare the inset of Figure 6b with the UV-vis DRS profile reported in Figure 1). This effect is less remarkable in the case of Au/D_12 (inset of Figure 6c).

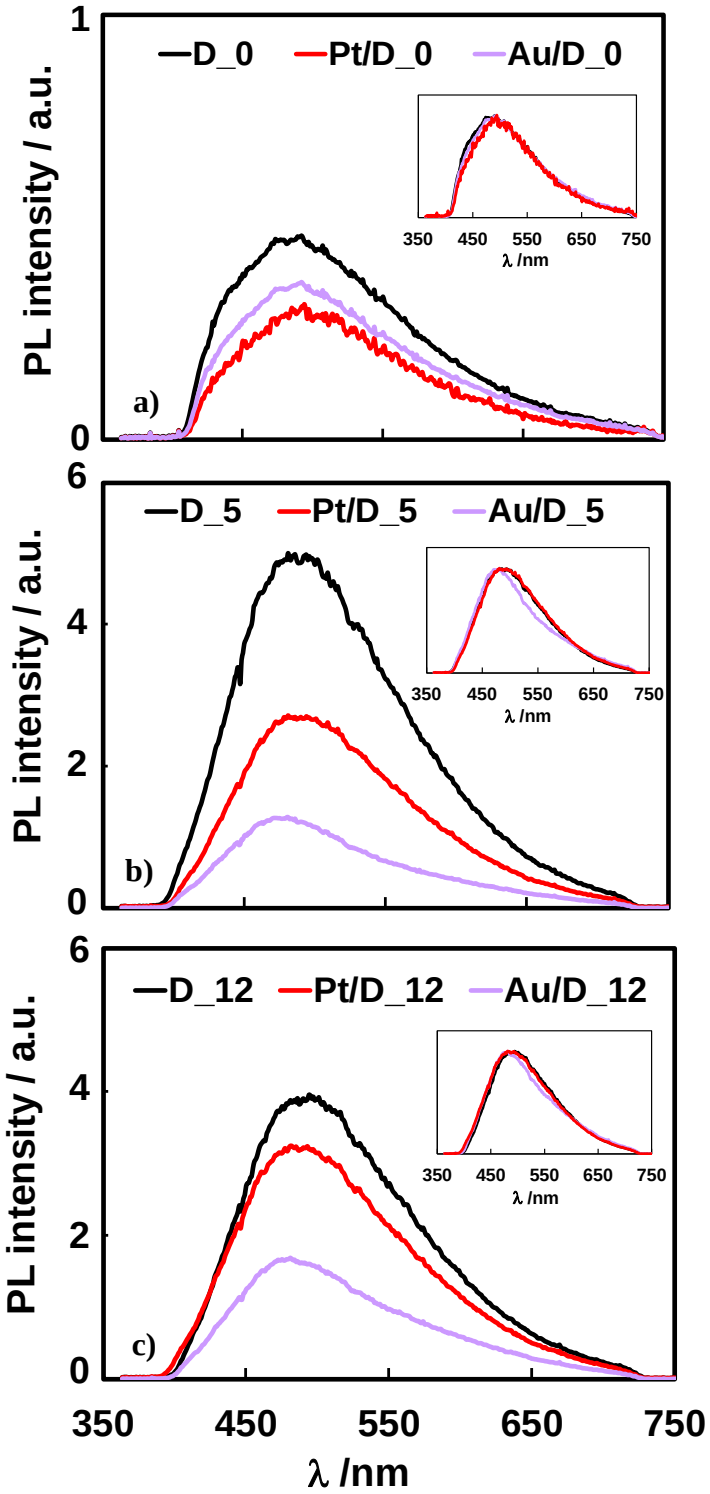

Figure 6. Photoluminescence spectra of the (a) NM/D_0, (b) NM/D_5 and (c) NM/D_12 sample series upon excitation at 355 nm. Inset: comparison among normalized PL spectra.

Therefore, Au NPs seem to be able not only to efficiently scavenge the electrons trapped at the TiO_2 defect sites, but also to (re)absorb PL photons with energy corresponding to their

plasmonic resonance. An extra PL quenching channel, due to energy transfer between photoexcited doped TiO_2 trap states and Au NPs, may thus occur.[41,42]

The overall extent of PL suppression induced by NM NPs was determined by calculating the ratio between the intensity of the steady state PL signal obtained with each NM-modified sample (indicated as S_{Au} or S_{Pt}) and that attained with the corresponding bare D_X TiO_2 material (defined as S). Interestingly, as shown in Figure 7, the S_{NM}/S ratios appear to inversely correlate to the corresponding relative photoactivity increase upon NM NPs deposition, in terms of the k_{NM}/k rate constants ratios (Figure 4). In particular, the most significant PL intensity reduction was attained upon Au NPs deposition on D_5 (S_{Au}/S = 0.25) and is accompanied by the highest increase (*ca.* × 5) in the k ratio, compared to D_0. Differently, the deposition of Pt NPs on D_5 did not produce a so marked PL intensity decrease (S_{Pt}/S = 0.50) and is accompanied by a relatively smaller photoactivity enhancement compared to D_0. In fact, the k ratio increased only by a factor *ca.* 2.5.

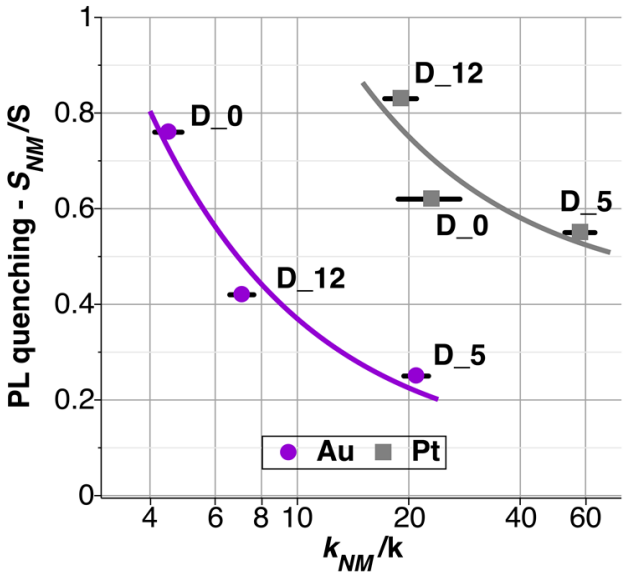

Figure 7. Correlation between the photoluminescence quenching degree (S_{NM}/S) and the corresponding photoactivity increase (k_{NM}/k) attained upon Au or Pt NPs deposition on either undoped or N,F co-doped TiO_2. The S_{NM}/S parameter corresponds to the ratio between the intensity of the steady state PL signal (*i.e.* integrated in the 400-750 nm range) obtained with each NM-modified sample (indicated as S_{Au} or S_{Pt}) and that attained with the corresponding bare D_X TiO_2 material (defined as S). k_{NM}/k values are collected in Figure 4.

The specific effects induced by NM NPs (*i.e.* especially in the case of Au) on the PL response of N,F-codoped materials can be also appreciated by comparing the PL decays exhibited by NM modified samples with those of the corresponding unmodified ones, as shown in Figure 8. In particular, Au NPs deposition on TiO_2 leads to a much faster decay, especially in the case of the D_5 series, while the effect of Pt NPs deposition is definitely smaller.

The triexponential decay fitting of the PL signal decay of all investigated materials (see section 2.3) led to the decay parameters reported in Table 3 and Table S1. The PL dynamics consists of a dominant very fast (1-2 ns) relaxation with amplitude A_1 and lifetime τ_1, related to the fast recombination of excitons, which is indeed overestimated by the convolution with the laser pulse, and a relatively longer-lasting emission, including two exponential decay components, with amplitudes A_2 and A_3 and lifetimes τ_2 and τ_3, respectively, the last one being in the order of tens of nanosecond.

Table 3. Parameters obtained by fitting the time resolved PL decay curves according to a tri-exponential decay equation.

sample	A_1 (%)	τ_1 (ns)	A_2 (%)	τ_2 (ns)	A_3 (%)	τ_3 (ns)
D_0	96.6	1.03	3.2	6.70	0.2	26.8
Au/D_0	96.2	1.02	3.6	6.61	0.2	27.2
Pt/D_0	96.4	1.03	3.4	6.19	0.2	23.5
D_5	89.4	1.61	9.4	8.87	1.2	32.5
Au/D_5	94.5	1.56	5.4	7.40	0.1	29.2
Pt/D_5	92.0	1.66	7.4	8.61	0.6	29.7
D_12	91.0	1.73	8.3	9.58	0.7	32.6
Au/D_12	91.9	1.63	7.5	8.64	0.6	29.7
Pt/D_12	89.9	1.79	9.1	9.62	1.0	31.9

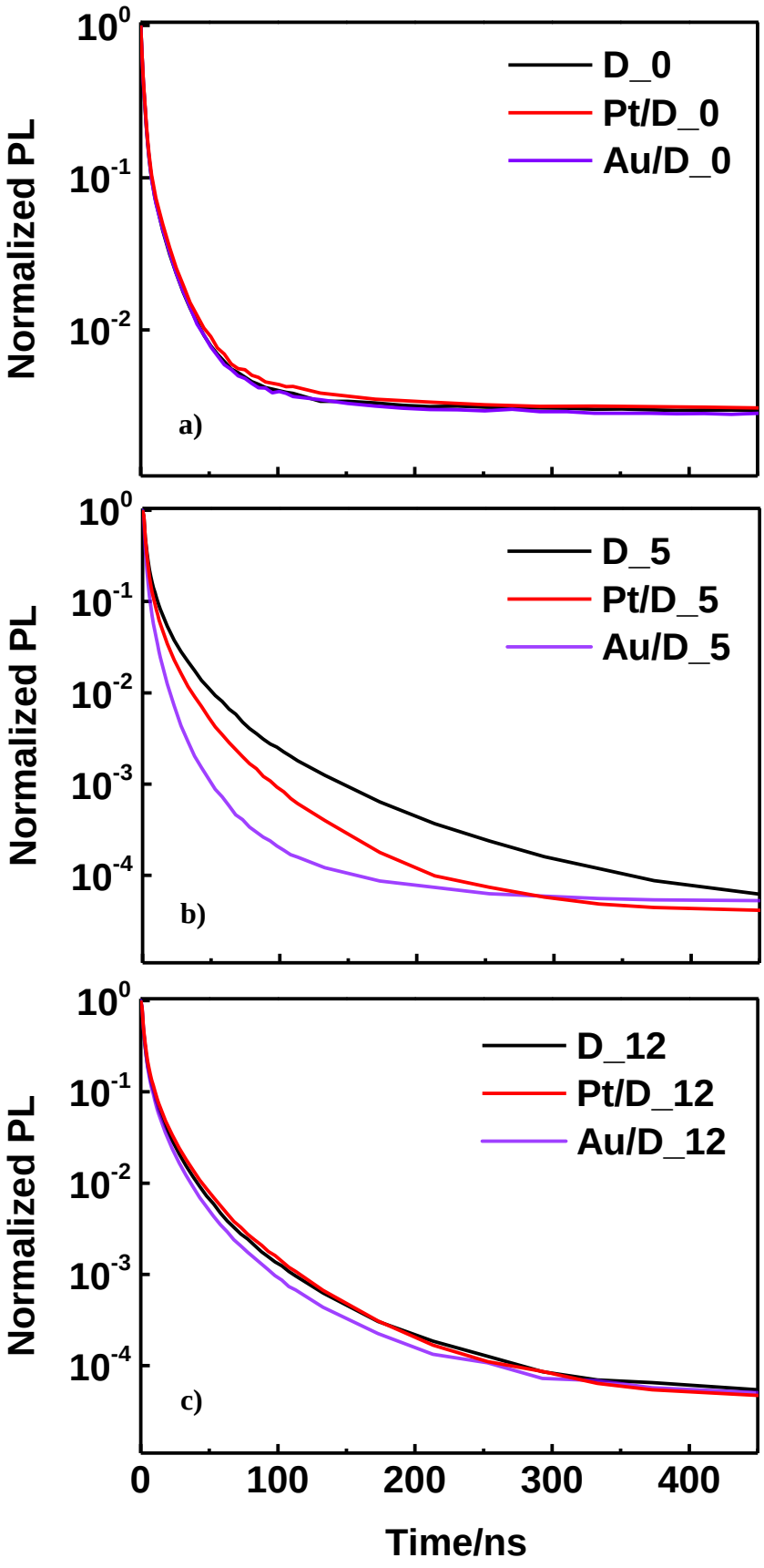

Figure 8. Photoluminescence decay measured for the (a) NM/D_0, (b) NM/D_5 and (c) NM/D_12 photocatalysts series.

The long living PL emission was ascribed to the presence of surface trap sites, stabilized by fluorine doping and relatively high calcination temperature (*i.e.* 700 °C), which, if present in optimal amount, were shown to have beneficial effects on the overall photoactivity of bare doped materials.[19] In addition, present results confirm that doping mainly affects the density of such trap states, which is correlated with A_2 and A_3 values. In fact, the sum of the A_2 and A_3 amplitudes accounts for a larger long living emission in the case of doped materials, the highest contribution of *ca.* 11% being attained with D_5, compared to the lowest 3.4% value observed in the case of D_0.

D_12 exhibits both a less intense PL emission (Figure 5) and a lower extent of the long-living PL component (A_2 and A_3) with respect to D_5. This may be a direct consequence of a too high amount of NH_4F dopant employed in its synthesis, which leads to an excess of defects in the oxide structure, mainly acting in this sample as rapid and detrimental recombination centers of photogenerated charge carriers.

As to the effects induced by the presence of NM NPs on the dynamics of the photogenerated charge carriers, we note, first of all, that NM NPs deposition seems to mainly affect the PL decay of D_5, as evidenced in Figure 8. In particular, Au NPs induce a marked decrease in the amplitude (A_3) respect to that of the lifetime (τ_3) associated to the slowest decaying PL component, A_2 being also partially affected. Thus, Au NPs seem to strongly interact with the electrons trapped at the defect sites. Consequently, the density of long-living electron-hole couples decreases by about one order of magnitude, as evidenced by comparing the A_3 value obtained for Au/D_5 to that obtained for D_5 (Table 3).

Interestingly, TiO_2 surface modification with Pt NPs does not produce such a strong variation in the amplitude of the long living PL emission, *i.e.* the transfer of photoexcited electrons from the CB of TiO_2 towards Pt NPs seems to be less affected by the defect trap sites introduced by doping. This might be a consequence of a different distribution of

photodeposited Pt NPs on the oxide surface, with respect to photodeposited Au NPs, for which a specific interaction with the trap states introduced by doping appears to be favored due to a different mechanism governing the growth of Pt respect to Au NPs during the photodeposition step on the oxide material. In fact, according to the electron portioning effect involved in the conventional photodeposition process,[43] gold NPs tend to nucleate and grow on the TiO_2 surface at oxygen-deficient titanium sites of high-electron density, which in the present case may correspond to the long living luminescent trap sites. Conversely, due to a different adsorption behavior of Pt ions and complexes from the solution onto the TiO_2 surface,[43] the density of nucleation sites for Pt NPs may be dissimilar from those available for gold and therefore a greater level of dispersion is expected for Pt NPs in comparison to Au NPs for the same nominal metal loading. Indeed, the HR-TEM images reported in Figures 2 and 3 fully confirm that photodeposited Pt NPs are smaller in size and much better dispersed on the TiO_2 surface than Au NPs.

The peculiar tendency of gold nanoclusters to grow on TiO_2 electron-rich defective sites, *i.e.* oxygen vacancies and and/or edge sites, is supported by scanning tunneling microscopy studies[44] and by a recent Raman investigation reporting a significant blue shift and broadening of TiO_2 Raman features only upon Au NPs photodeposition. This confirms a predominant interaction between defective titania and gold NPs, which instead appears to be lower in the case of Pt NPs.[45] The expected proximity of Au NPs to the long-living surface defect sites induced by N,F doping of TiO_2 is indirectly supported also by the here performed HR-TEM analysis. In fact Figures 2a,b and 3a,b clearly show that, with respect to undoped Au/D_0, Au/D_5 is characterized by a larger number of smaller Au NPs, reasonably grown on such electron trap states during photodeposition.

Thus, as sketched in Scheme 1, the electrons photopromoted to the CB of N,F-doped TiO_2 modified by Au or Pt NPs, besides directly recombining with VB holes on the subnanosecond

time scale, may undergo different transfer paths, *i.e.* they may be scavenged by NM NPs either directly (*route a*), or after being trapped at the defect sites introduced by doping (*routes b-c*). The electrons at the trap sites may then recombine with VB holes, either non-radiatively, or producing the typical long-living radiative emission (*route d*). In NM-containing TiO_2 samples this signal is obviously less intense than that recorded with the corresponding bare TiO_2. On the other hand, the electrons efficiently transferred to the NM NPs may relax via a non-radiative process[36] or be transferred to adsorbed substrate species during photocatalytic processes in the presence of efficient hole scavengers.

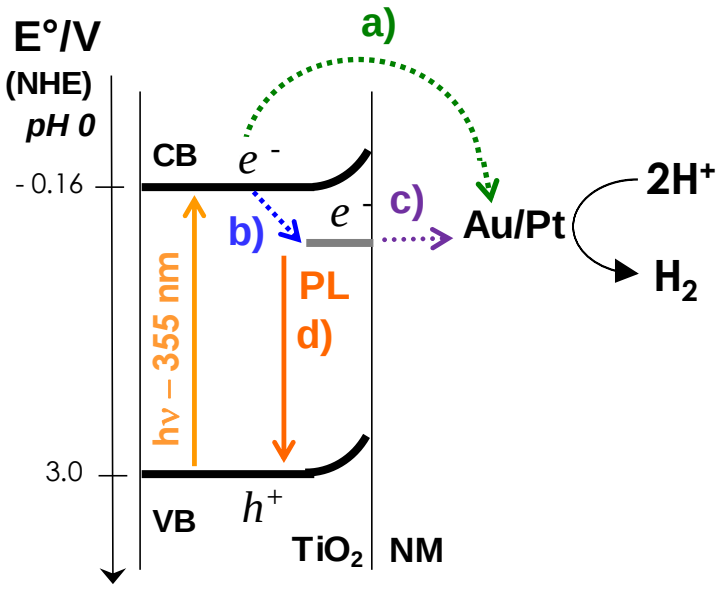

Scheme 1. Electron transfer paths occurring at NM (Au or Pt) NPs modified N,F-doped TiO_2. The grey line below the CB indicates the energy level of specific TiO_2 defect sites (induced by N,F-doping and calcination at 700 °C), from which the long-lasting PL signal originates. Straight and dotted lines indicate radiative and non radiative transitions, respectively.

By considering the PL signal decrease recorded with NM NPs-modified doped or undoped materials (Figure 6), Au rather than Pt NPs appear to be able to efficiently capture electrons trapped at defect sites, possibly because of their close proximity due to their specific nucleation and growth during photodeposition.[43] Differently, Pt NPs seem to be less prone to

depopulate such electron trap states, probably because of their more broad distribution on the TiO_2 surface.

The relatively more marked increase of photoactivity in H_2 production attained by combining N,F-doping of TiO_2 with its surface modification by Au NPs photodeposition can thus be explained. In fact, in the so obtained materials also part of the electrons trapped in defect sites may become available for proton reduction on the NM NPs, where H_2 evolution efficiently occurs.

Differently, in the case of Pt/D_X photocatalysts, minor, if any, electron transfer from trap sites to Pt NPs occurs (*route c* in Scheme 1). Indeed, a larger amount of photoexcited electrons may survive at defect trapping sites and undergo radiative recombination with VB holes (*route d* in Scheme 1). This accounts for the smaller PL intensity decrease observed for Pt/D_X samples with respect to the corresponding Au/D_X materials.

By this way the clear correlation outlined in Figure 7 between the PL signal decrease in NM-containing photocatalysts and the photoactivity increase in H_2 production is fully explained. A lower population of luminescent trap states is obtained in NM-containing samples with respect to the corresponding bare ones, and this is more remarkable in the case of Au-containing samples, because in this case electron transfer is boosted from the trap luminescent states to Au NPs where H_2 formation occurs (*route c* in Scheme 1).

On the other hand, the fact that Pt is a more efficient co-catalyst than gold in photocatalytic hydrogen production is a consequence of the more efficient direct electron transfer from the CB of TiO_2 to Pt, rather than to Au NPs, due to the relatively higher work function of Pt.[46,47] Consequently, all Pt-modified photocatalysts exhibit the highest activity in photocatalytic H_2 production, the relative rate constants being $k_{Pt} > k_{Au} > k$ for each series of samples.

The fact that Pt NPs intrinsically are most efficient in capturing CB electrons is confirmed by the high photoactivity improvement attained upon Pt NPs photodeposition on D_0, leading to a k_{Pt}/k ratio of *ca.* 23, as shown in Figure 4. However, in the case of D_5, containing an optimal amount of surface trap states, the k_{Pt}/k ratio is only *ca.* 2.5-fold larger than the k_{Pt}/k ratio for D_0, to be compared to the *ca.* 5 k_{Au}/k ratio enhancement factor obtained for Au/D_5 with respect to the relatively low k_{Au}/k ratio obtained for Au/D_0. Thus platinum is a better co-catalyst than gold, but gold exhibits a larger synergistic effect when photodeposited on surface trap states containing TiO_2.

4. CONCLUSIONS

PL measurements allow to clarify how NM NPs may differently interact with the electrons photopromoted in anatase N,F-doped TiO_2 materials, thus contributing to the overall electron-hole couples separation through different paths. The here evidenced interaction between Au NPs and the long-living PL originating surface traps may be at the origin of the extra positive contribution that N,F-doping of TiO_2 provides to the beneficial effect produced by NM NPs photodeposition on TiO_2, particularly in the photoreduction path leading to H_2 production.[20]

Time-resolved PL spectroscopy thus confirms to be a powerful and complementary analysis tool for determining not only the presence of specific trap states in semiconductor oxides influencing the dynamics of photogenerated carriers, but also their specific interaction with other surface species, *e.g.* NM NPs, for a better understanding of the different mechanisms governing the overall efficiency of photocatalytic materials.[8]

ASSOCIATED CONTENT

Supporting Information. Main scheme of the set-up employed during time resolved photoluminescence (PL) experiments; examples of PL profile decay fitting curves; parameters obtained from time resolved PL decay curves according to a tri-exponential decay; time courses of the photocatalytic hydrogen production obtained with the investigated samples; ratios between the zero-order rate constants obtained with NM-D_X samples and that obtained with the corresponding D_X sample in the photocatalytic mineralization of formic acid. This material is available free of charge via the Internet at http://pubs.acs.org.

AUTHOR INFORMATION

Corresponding Author

* Phone: +39 02 50314298. Fax: +39 02 50314300. E-mail: mariavittoria.dozzi@unimi.it

Notes

The authors declare no competing financial interest.

ACKNOWLEDGMENTS

This work received financial support from Cariplo Foundation through the 2013-0615 grant to the project Novel Photocatalytic Materials Based on Heterojunctions for Solar Energy Conversion and from the Italian MIUR, through the PRIN 2015 SMARTNESS (2015K7FZLH) project. MVD acknowledges the financial support of the University of Milano through the project PSR2017_DIP_005_-_DOZZI "Piano di Sostegno alla Ricerca 2015/2017, linea 2, Azione A".

REFERENCES

(1) Schneider, J.; Matsuoka, M.; Takeuchi, M.; Zhang, J.; Horiuchi, Y.; Anpo, M.; Bahnemann, D. W. Understanding TiO_2 Photocatalysis: Mechanisms and Materials. *Chem. Rev.* **2014**, *114*, 9919–9986.

(2) Kumar, S. G.; Rao, K. S. R. K. Comparison of Modification Strategies towards Enhanced Charge Carrier Separation and Photocatalytic Degradation Activity of Metal Oxide Semiconductors (TiO_2, WO_3 and ZnO). *Appl. Surf. Sci.* **2017**, *391*, 124–148.

(3) Park, H.; Park, Y.; Kim, W.; Choi, W. Surface Modification of TiO_2 Photocatalyst for Environmental Applications. *J. Photochem. Photobiol. C Photochem. Rev.* **2013**, *15*, 1–20.

(4) Dozzi, M. V.; Ohtani, B.; Selli, E. Absorption and Action Spectra Analysis of Ammonium Fluoride-Doped Titania Photocatalysts. *Phys. Chem. Chem. Phys.* **2011**, *13*, 18217–18227.

(5) Dozzi, M. V.; Selli, E. Doping TiO_2 with p-Block Elements: Effects on Photocatalytic Activity. *J. Photochem. Photobiol. C Photochem. Rev.* **2013**, *14*, 13–28.

(6) Linsebigler, A. L.; Linsebigler, A. L.; Yates Jr, J. T.; Lu, G.; Lu, G.; Yates, J. T. Photocatalysis on TiO_2 Surfaces: Principles, Mechanisms, and Selected Results. *Chem. Rev.* **1995**, *95*, 735–758.

(7) Minato, T.; Susaki, T.; Shiraki, S.; Kato, H. S.; Kawai, M.; Aika, I., K. Investigation of the Electronic Interaction between TiO2 (110) Surfaces and Au Clusters by PES and STM. *Surf. Sci.* **2004**, *566–568*, 1012−1017.

(8) Luo, C.; Ren, X.; Dai, Z.; Zhang, Y.; Qi, X.; Pan, C. Present Perspectives of Advanced Characterization Techniques in TiO_2-Based Photocatalysts. *ACS Appl. Mater. Interfaces* **2017**, *9*, 23265–23286.

(9) Pallotti, D. K.; Passoni, L.; Maddalena, P.; Di Fonzo, F.; Lettieri, S. Photoluminescence Mechanisms in Anatase and Rutile TiO_2. *J. Phys. Chem. C* **2017**, *121*, 9011–9021.

(10) Vequizo, J. J. M.; Kamimura, S.; Ohno, T.; Yamakata, A. Oxygen Induced Enhancement of NIR Emission in Brookite TiO_2 Powders: Comparison with Rutile and Anatase TiO_2 Powders. *Phys. Chem. Chem. Phys.* **2018**, *20*, 3241–3248.

(11) Yamada, Y.; Kanemitsu, Y. Determination of Electron and Hole Lifetimes of Rutile and Anatase TiO_2 Single Crystals. *Appl. Phys. Lett.* **2012**, *101*, 133907.

(12) Rex, R. E.; Knorr, F. J.; McHale, J. L. Surface Traps of TiO_2 Nanosheets and Nanoparticles as Illuminated by Spectroelectrochemical Photoluminescence. *J. Phys. Chem. C* **2014**, *118*, 16831–16841.

(13) Rex, R. E.; Knorr, F. J.; McHale, J. L. Imaging Luminescent Traps on Single Anatase TiO_2 Crystals: The Influence of Surface Capping on Photoluminescence and Charge Transport. *J. Phys. Chem. C* **2015**, *119*, 26212–26218.

(14) Shi, J.; Chen, J.; Feng, Z.; Chen, T.; Lian, Y.; Wang, X.; Li, C. Photoluminescence Characteristics of TiO_2 and Their Relationship to the Photoassisted Reaction of Water/Methanol Mixture. *J. Phys. Chem. C* **2007**, *111*, 693–699.

(15) Knorr, F. J.; Zhang, D.; McHale, J. L. Influence of $TiCl_4$ Treatment on Surface Defect Photoluminescence in Pure and Mixed-Phase Nanocrystalline TiO_2. *Langmuir* **2007**,

23, 8686–8690.

(16) McEntee, M.; Stevanovic, A.; Tang, W.; Neurock, M.; Yates, J. T. Electric Field Changes on Au Nanoparticles on Semiconductor Supports - The Molecular Voltmeter and Other Methods to Observe Adsorbate-Induced Charge-Transfer Effects in Au/TiO_2 Nanocatalysts. *J. Am. Chem. Soc.* **2015**, *137*, 1972–1982.

(17) Stevanovic, A.; Büttner, M.; Zhang, Z.; Yates, J. T. Photoluminescence of TiO_2: Effect of UV Light and Adsorbed Molecules on Surface Band Structure. *J. Am. Chem. Soc.* **2012**, *134*, 324–332.

(18) Ma, S.; Reish, M. E.; Zhang, Z.; Harrison, I.; Yates, J. T. Anatase-Selective Photoluminescence Spectroscopy of P25 TiO_2 Nanoparticles: Different Effects of Oxygen Adsorption on the Band Bending of Anatase. *J. Phys. Chem. C* **2017**, *121*, 1263–1271.

(19) Dozzi, M. V.; D'Andrea, C.; Ohtani, B.; Valentini, G.; Selli, E. Fluorine-Doped TiO_2 Materials : Photocatalytic Activity vs Time-Resolved Photoluminescence. *J. Phys. Chem. C* **2013**, *117*, 25586–25595.

(20) Dozzi, M. V.; Saccomanni, A.; Altomare, M.; Selli, E. Photocatalytic Activity of NH_4F-Doped TiO_2 Modified by Noble Metal Nanoparticle Deposition. *Photochem. Photobiol. Sci.* **2013**, *12*, 595–601.

(21) Dozzi, M. V.; Livraghi, S.; Giamello, E.; Selli, E. Photocatalytic Activity of S- and F-Doped TiO_2 in Formic Acid Mineralization. *Photochem. Photobiol. Sci.* **2011**, *10*, 343–349.

(22) Dozzi, M. V.; Prati, L.; Canton, P.; Selli, E. Effects of Gold Nanoparticles Deposition on the Photocatalytic Activity of Titanium Dioxide under Visible Light. *Phys. Chem. Chem. Phys.* **2009**, *11*, 7171–7180.

(23) Dozzi, M. V.; Saccomanni, A.; Selli, E. Cr(VI) Photocatalytic Reduction: Effects of Simultaneous Organics Oxidation and of Gold Nanoparticles Photodeposition on TiO_2. *J. Hazard. Mater.* **2012**, *211*, 188–195.

(24) Chiarello, G. L.; Aguirre, M. H.; Selli, E. Hydrogen Production by Photocatalytic Steam Reforming of Methanol on Noble Metal-Modified TiO_2. *J. Catal.* **2010**, *273*, 182–190.

(25) Artesani, A.; Bellei, S.; Capogrosso, V.; Cesaratto, A.; Mosca, S.; Nevin, A.; Valentini, G.; Comelli, D. Photoluminescence Properties of Zinc White: An Insight into Its Emission Mechanisms through the Study of Historical Artist Materials. *Appl. Phys. A Mater. Sci. Process.* **2016**, *122*, 1–11.

(26) Kowalska, E.; Abe, R.; Ohtani, B. Visible Light-Induced Photocatalytic Reaction of Gold-Modified Titanium(IV) Oxide Particles: Action Spectrum Analysis. *Chem. Commun.* **2009**, 241–243.

(27) Kowalska, E.; Mahaney, O. O. P.; Abe, R.; Ohtani, B. Visible-Light-Induced Photocatalysis through Surface Plasmon Excitation of Gold on Titania Surfaces. *Phys. Chem. Chem. Phys.* **2010**, *12*, 2344–2355.

(28) Chiarello, G. L.; Ferri, D.; Selli, E. Effect of the CH_3OH/H_2O Ratio on the Mechanism of the Gas-Phase Photocatalytic Reforming of Methanol on Noble Metal-Modified TiO_2. *J. Catal.* **2011**, *280*, 168–177.

(29) Emeline, A. V.; Ryabchuk, V. K.; Serpone, N. Dogmas and Misconceptions in

Heterogeneous Photocatalysis. Some Enlightened Reflections. *J. Phys. Chem. B* **2005**, *109*, 18515–18521.

(30) Zhang, Z.; Lin, Q.; Kurunthu, D.; Wu, T.; Zuo, F.; Zheng, S. T.; Bardeen, C. J.; Bu, X.; Feng, P. Synthesis and Photocatalytic Properties of a New Heteropolyoxoniobate Compound: $K_{10}[Nb_2O_2(H_2O)_2][SiNb_{12}O_{40}]\cdot 12H_2O$. *J. Am. Chem. Soc.* **2011**, *133*, 6934–6937.

(31) Tang, H.; Berger, H.; Schmid, P. E.; Levy, F. Photoluminescence in TiO_2 Anatase Single Crystals. *Solid State Commun.* **1993**, *87*, 847− 850.

(32) Hosaka, N.; Sekiya, T.; Kurita, S. Excitonic State in Anatase TiO_2 Single Crystal. *J. Lumin.* **1997**, *72*, 874−875.

(33) Watanabe, M.; Sasaki, S.; Hayashi, T. Time-Resolved Study of Photoluminescence in Anatase TiO_2. *J. Lumin.* **2000**, *87–89*, 1234−1236.

(34) Serpone, N.; Lawless, D.; Khairutdinov, R. Size Effects on the Photophysical Properties of Colloidal Anatase TiO_2 Particles: Size Quantization versus Direct Transitions in This Indirect Semiconductor? *J. Phys. Chem.* **1995**, *99*, 16646–16654.

(35) Wang, Y.; Zhang, H.; Liu, P.; Sun, T.; Li, Y.; Yang, H.; Yao, X.; Zhao, H. Nature of Visible-Light Responsive Fluorinated Titanium Dioxides. *J. Mater. Chem. A* **2013**, *1*, 12948−12953.

(36) Stevanovic, A.; Ma, S.; Yates, J. T. Effect of Gold Nanoparticles on Photoexcited Charge Carriers in Powdered TiO_2-Long Range Quenching of Photoluminescence. *J. Phys. Chem. C* **2014**, *118*, 21275–21280.

(37) Sofianou, M. V.; Boukos, N.; Vaimakis, T.; Trapalis, C. Decoration of TiO_2 Anatase Nanoplates with Silver Nanoparticles on the {101} Crystal Facets and Their Photocatalytic Behaviour. *Appl. Catal. B Environ.* **2014**, *158–159*, 91–95.

(38) Devaraji, P.; Sathu, N. K.; Gopinath, C. S. Ambient Oxidation of Benzene to Phenol by Photocatalysis on $Au/Ti_{0.98}V_{0.02}O_2$: Role of Holes. *ACS Catal.* **2014**, *4*, 2844–2853.

(39) Shao, Z. F.; Yang, Y. Q.; Liu, S. T.; Wang, Q. Transient Competition between Photocatalysis and Carrier Recombination in TiO_2 Nanotube Film Loaded with Au Nanoparticles. *Chinese Phys. B* **2014**, *23*, 0961021–0961028.

(40) Majumder, S.; Jana, S. K.; Bagani, K.; Satpati, B.; Kumar, S.; Banerjee, S. Fluorescence Resonance Energy Transfer and Surface Plasmon Resonance Induced Enhanced Photoluminescence and Photoconductivity Property of Au-TiO_2 Metal-Semiconductor Nanocomposite. *Opt. Mater. (Amst).* **2015**, *40*, 97–101.

(41) Zhang, X.; Marocico, C. A.; Lunz, M.; Gerard, V. A.; Gun'Ko, Y. K.; Lesnyak, V.; Gaponik, N.; Susha, A. S.; Rogach, A. L.; Bradley, A. L. Wavelength, Concentration, and Distance Dependence of Nonradiative Energy Transfer to a Plane of Gold Nanoparticles. *ACS Nano* **2012**, *6*, 9283–9290.

(42) Viste, P.; Plain, J.; Jaffiol, R.; Vial, A.; Adam, P. M.; Royer, P. Enhancement and Quenching Regimes in Metal-Semiconductor Hybrid Optical Nanosources. *ACS Nano* **2010**, *4*, 759–764.

(43) Kydd, R.; Chiang, K.; Scott, J.; Amal, R. Low Energy Photosynthesis of Gold-Titania Catalysts. *Photochem. Photobiol. Sci.* **2007**, *6*, 829–832.

(44) Gong, X. Q.; Selloni, A.; Dulub, O.; Jacobson, P.; Diebold, U. Small Au and Pt Clusters at the Anatase TiO_2(101) Surface: Behavior at Terraces, Steps, and Surface

Oxygen Vacancies. *J. Am. Chem. Soc.* **2008**, *130*, 370–381.

(45) Melvin, A. A.; Illath, K.; Das, T.; Raja, T.; Bhattacharyya, S.; Gopinath, C. S. M–Au/TiO_2 (M = Ag, Pd, and Pt) Nanophotocatalyst for Overall Solar Water Splitting: Role of Interfaces. *Nanoscale* **2015**, *7*, 13477–13488.

(46) Anpo, M.; Takeuchi, M. The Design and Development of Highly Reactive Titanium Oxide Photocatalysts Operating under Visible Light Irradiation. *J. Catal.* **2003**, *216*, 505–516.

(47) Naldoni, A.; D'Arienzo, M.; Altomare, M.; Marelli, M.; Scotti, R.; Morazzoni, F.; Selli, E.; Dal Santo, V. Pt and Au/TiO_2 Photocatalysts for Methanol Reforming: Role of Metal Nanoparticles in Tuning Charge Trapping Properties and Photoefficiency. *Appl. Catal. B Environ.* **2013**, *130–131*, 239–248.

TOC